



# Reactive Dye Adsorption from Aqueous Solution on HPEI-Modified Fe<sub>3</sub>O<sub>4</sub> Nanoparticle as a Superadsorbent: Characterization, Modeling, and Optimization

Arash Dalvand<sup>1,2</sup> · Mehdi Khoobi<sup>3,4</sup> · Ramin Nabizadeh<sup>2</sup> · Mohammad Reza Ganjali<sup>5,6</sup> · Elham Gholibegloo<sup>7</sup> · Amir Hossein Mahvi<sup>8,9,10</sup>

Published online: 4 April 2018  
© Springer Science+Business Media, LLC, part of Springer Nature 2018

## Abstract

In this work, the optimum condition for the adsorption of Reactive Blue 19 dye onto Fe<sub>3</sub>O<sub>4</sub> functionalized with hyperbranched polyethylenimine (Fe@HPEI) was determined using response surface methodology. The properties of synthesized magnetic Fe@HPEI nanoparticles were ascertained using FTIR, SEM, TEM, VSM and zeta potential measurement. The experimental adsorption data indicating the positive effect of adsorbent dose and contact time, and the negative effect of pH, initial dye concentration and ionic strength on dye adsorption. At optimal condition; pH 3.4, contact time 25 min, adsorbent dose 0.4 g/L and initial dye concentration 113 mg/L, Fe@HPEI nanoparticles removed dye up to 99.27%. The maximum experimental dye adsorption was near to the predicted value of 100%, which confirmed the reliability of the selected statistical model. The dye adsorption data were fitted well to Langmuir isotherm and pseudo-second-order kinetic, and the maximum adsorption capacity was 500 mg/g. Totally, Fe@HPEI as an effective superadsorbent can be repeatedly utilized for the adsorption of dye from the aqueous environment.

**Keywords** Dye adsorption · Fe@HPEI · Central composite design · Modeling · Optimization

## Introduction

There are more than 10,000 commercial synthetic dyes [1, 2] which are widely applied in a wide range of industries [3–5]. Synthetic dyes have different classes, but the reactive

dyes are the most common dyes which are employed in textile industries [6, 7]. It has been estimated about 10–50% of reactive dyes that have utilized in dyeing processes enter the wastewater [8, 9]. Since the most of reactive dyes have complex structure [10] and are resistant to biological

✉ Amir Hossein Mahvi  
ahmahvi@yahoo.com

<sup>1</sup> Environmental Science and Technology Research Center, Department of Environmental Health Engineering, School of Public Health, Shahid Sadoughi University of Medical Sciences, Yazd, Iran

<sup>2</sup> Department of Environmental Health Engineering, School of Public Health, Tehran University of Medical Sciences, Tehran, Iran

<sup>3</sup> Medical Biomaterials Research Center, Tehran University of Medical Sciences, Tehran, Iran

<sup>4</sup> Department of Medicinal Chemistry, Faculty of Pharmacy and Pharmaceutical Sciences Research Center, Tehran University of Medical Sciences, Tehran 14176, Iran

<sup>5</sup> Center of Excellence in Electrochemistry, Faculty of Chemistry, University of Tehran, Tehran, Iran

<sup>6</sup> Biosensor Research Center, Endocrinology and Metabolism Molecular-Cellular Sciences Institute, Tehran University of Medical Sciences, Tehran, Iran

<sup>7</sup> Department of Organic Chemistry, University of Zanjan, Zanjan, Iran

<sup>8</sup> Center for Water Quality Research, Institute for Environmental Research, Tehran University of Medical Sciences, Tehran, Iran

<sup>9</sup> Center for Solid Waste Research, Institute for Environmental Research, Tehran University of Medical Sciences, Tehran, Iran

<sup>10</sup> National Institute of Health Research, Tehran University of Medical Sciences, Tehran, Iran

degradation, discharge of textile wastewater containing synthetic dyes into the water bodies is harmful to the environment [11, 12]. Reactive Blue 19 (RB 19) dye [13], which is widely employed in textile industries, has toxic and recalcitrant nature [14]. Owing to the existence of two sulfonate groups in the chemical structure of RB 19, it has anionic character.

Among various wastewater treatment techniques which have been utilized for dye removal, adsorption has advantages including; easy to design and operate, economic choice, and high efficiency for dye removal [15, 16]. In recent years, magnetic nanoparticles due to the virtues such as, biocompatibility [17], chemical stability, large surface area [18], low cost, easy separation and versatility in surface modification, have been modified with different chemicals containing amine groups, such as aminoguanidine [19], L-arginine [20], and lysine [21] and successfully employed for dye adsorption. Hyperbranched polyethyleneimine (HPEI) as an amine-rich polymer containing primary, secondary and tertiary amine groups in the approximate ratio of 1:2:1 has high cationic charge density [22, 23]. In previous studies conducted by other researchers, polyethylenimine has been applied for functionalization of different adsorbents, such as oil palm empty fruit bunch fibres [24], anaerobic granular sludge [25], polyvinyl chloride [26], and SiO<sub>2</sub> [27] and favourably used for adsorption of different dyes. Till now, no studies have been carried out on the application of Fe@HPEI for RB 19 dye removal. Thus, this paper aimed to study the efficiency of prepared Fe@HPEI for RB 19 dye adsorption. In parallel, the effect of different operational parameters on dye removal was investigated using central composite design (CCD), and a suitable statistical model for prediction of dye adsorption in various condition was presented.

## Experimental

### Materials

NH<sub>4</sub>OH (25%), FeSO<sub>4</sub>·7H<sub>2</sub>O, FeCl<sub>3</sub>·6H<sub>2</sub>O, HCl, NaOH·NaCl, and [3-(2,3-epoxypropoxy)propyl] trimethoxysilane (EPO) were provided from Merck (Germany). Hyperbranched polyethyleneimine (HPEI, molecular weight: 60,000 g/mol) was supplied from Sigma–Aldrich. RB 19 was from CIBA. The chemical structure of RB 19 is presented in Fig. 1.

### Characterization and Analysis

The images of adsorbent were taken by Field Emission scanning electron microscope (Mira 3 Tescan, Czech Republic) and transmission electron microscope (TEM). The Zeta

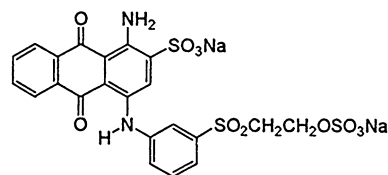


Fig. 1 The chemical structure of Reactive Blue 19 dye

potential of adsorbent (before and after dye adsorption) and dye solution was determined using zeta potential analyzer (Malvern, ZEN 3600, UK). A Fourier transformed infrared (FTIR) spectrometer (Perkin Elmer, USA) was utilized to record the Infra-red spectrum of adsorbent. A vibrating sample magnetometer (Magnetic Daghigh Daneshpajouh Co, Iran) was used to determine the magnetic properties of Fe<sub>3</sub>O<sub>4</sub> and Fe@HPEI. The RB 19 dye concentration was measured at maximum absorption wavelength of 592 nm using a UV–Vis spectrophotometer (Perkin Elmer, lambda 25, USA).

### Preparation of Fe<sub>3</sub>O<sub>4</sub>

Fe<sub>3</sub>O<sub>4</sub> magnetite nanoparticles were prepared by the chemical co-precipitation procedure [20]. Firstly, 0.6 g FeSO<sub>4</sub>·4H<sub>2</sub>O and 1.17 g FeCl<sub>3</sub>·6H<sub>2</sub>O were poured into 50 mL deionized water. The mixture was stirred for 30 min under nitrogen gas at 70 °C. Then, 10 mL NH<sub>4</sub>OH (25%) was added to the mixture and stirred for 1.5 h. An external magnet was used to separate the produced precipitates from the solution. The final black product was washed with deionised water five times and dried in an oven at 50 °C for 24 h.

### Grafting of HPEI onto Fe<sub>3</sub>O<sub>4</sub> (Fe@HPEI)

HPEI was grafted onto Fe<sub>3</sub>O<sub>4</sub> according to the following steps. 2 g of HPEI was added to 200 mL dry toluene. Then, 0.63 g EPO was poured into the mixture and agitated for 24 h at 80 °C. Well-dispersed 2.5 g Fe<sub>3</sub>O<sub>4</sub> in 25 mL ethanol were then added, and the resultant mixture was stirred at 80 °C for 24 h. The final black product was isolated by an external magnet and washed with ethanol for five times to remove unreacted chemicals. Finally, the prepared Fe@HPEI magnetic nanoparticles were dried in an oven at 50 °C overnight. The sequence of Fe@HPEI preparation is schematically illustrated in Fig. 2.

### Adsorption Procedure

In each adsorption test a predetermined dose of Fe@HPEI was added to a 100 mL Erlenmeyer flask containing a specific amount of dye and the pH was set to 3, 5, 7, 9 or 11 by using HCl (0.1 M) or NaOH (0.1 M), and the solution

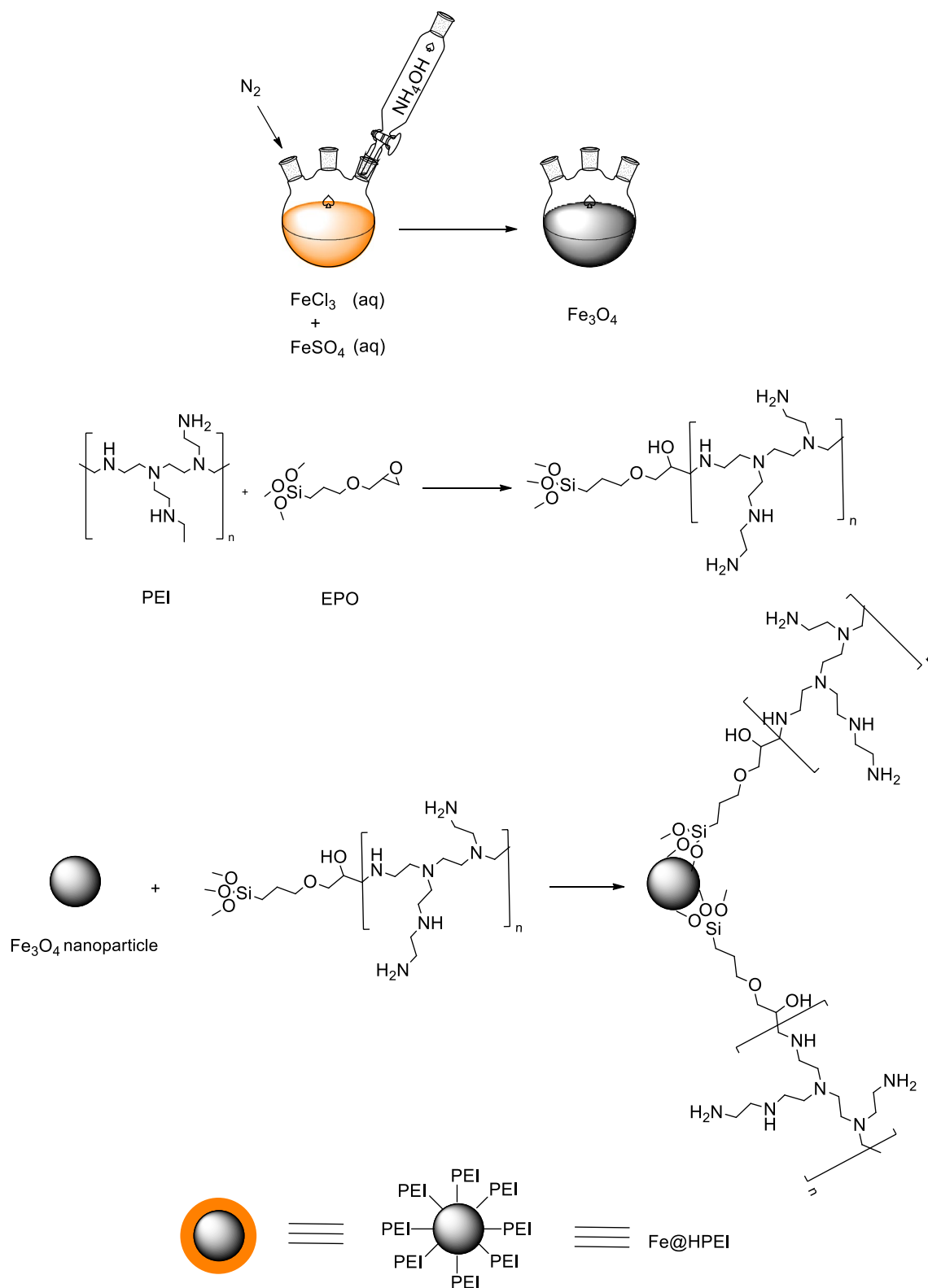


**Fig. 2** Schematic illustration of synthesis processes for preparation of Fe@HPEI

was agitated at rapid speed of 200 RPM for 2, 9, 16, 23 or 30 min. A permanent magnet was applied to separate adsorbent from the solution after shaking, and the RB 19 concentration in solution was determined by spectrophotometer.

## Design of Experiments

To investigate the effect of different operational parameters on the adsorption of RB 19 dye, four parameters of adsorbent dose, pH, contact time, and initial dye concentration with five levels for each one were chosen (Table 1). Design Expert software (version 7, trial, Stat-Ease) was applied for designing the experiments (based on CCD) and analysing the obtained data. The response surface regression was utilized for analysing the experimental results, and the optimal condition for dye adsorption was approximated by a second-order polynomial model as given by Eq. (1):

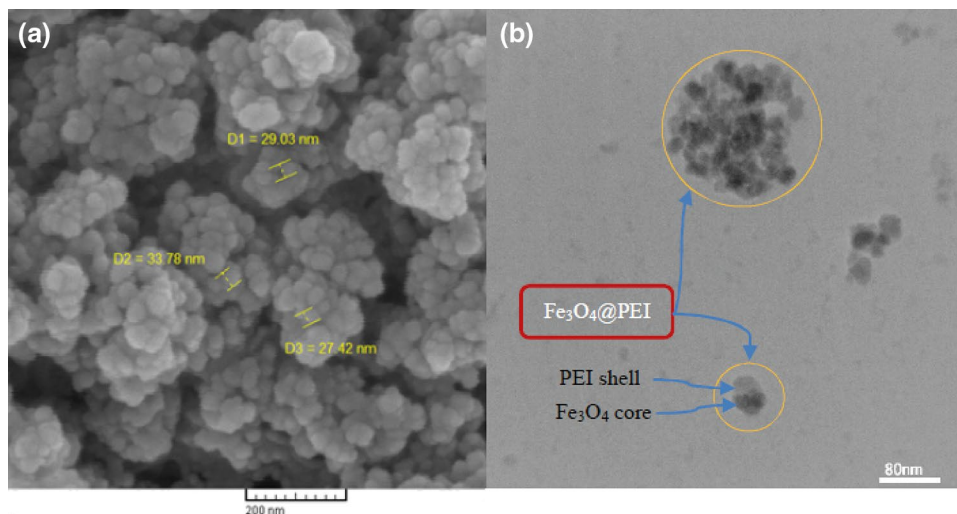
$$Y = \beta_0 + \sum_{i=1}^k \beta_i X_i + \sum_{i=1}^k \beta_{ii} X_i^2 + \sum_{i=1}^k \sum_{j=1}^k \beta_{ij} X_i X_j + \varepsilon \quad (1)$$

where  $Y$  is the predicted dye adsorption (%);  $\beta_0$  is the model constant coefficient,  $X_i$  and  $X_j$  are the coded variables.  $\beta_i$ ,  $\beta_{ii}$  and  $\beta_{ij}$  are the linear, quadratic and interaction model coefficients, respectively.

**Table 1** Levels of variables studied in central composite design

Variable	Unit	Coded symbol	Levels				
			$-\alpha$	$-1$	$0$	$1$	$+\alpha$
pH	–	A	3	5	7	9	11
Adsorbent dose	g/L	B	0.1	0.2	0.3	0.4	0.5
Time	min	C	2	9	16	23	30
Dye concentration	mg/L	D	20	65	110	155	200

**Fig. 3** a SEM, and b TEM images of Fe@HPEI



## Results and Discussion

### Characterization of Fe@HPEI

#### FE-SEM and TEM Analysis

Field emission scanning electron microscope (FE-SEM) and TEM were used to evaluate the morphology and size of prepared  $\text{Fe}_3\text{O}_4$  nanoparticles functionalized by HPEI.

As shown in Fig. 3a, all of Fe@HPEI magnetic nanoparticles are almost the same size and shape. By analysing the FE-SEM image, it could be understood that Fe@HPEI nanoparticles have the average size of 20–35 nm. TEM image (Fig. 3b) indicates that  $\text{Fe}_3\text{O}_4$  nanoparticles have favorably been covered by HPEI.

#### FTIR Analysis

Figure 4 depicts the FTIR spectra of the Fe@HPEI. As illustrated in this figure, the band at  $584\text{ cm}^{-1}$  is due to Fe–O bond. The peaks at  $1022\text{--}1114\text{ cm}^{-1}$  are assigned to Si–O–H and Si–O–Si groups [28]. The band at  $1457$  corresponds to the aliphatic C–H bending vibrations; while the peaks at  $2834$ , and  $2951\text{ cm}^{-1}$  are related to asymmetric and symmetric stretching vibrations of  $-\text{CH}_2-$  in the structure of HPEI. The strong band at  $3419\text{ cm}^{-1}$  can be attributed to N–H

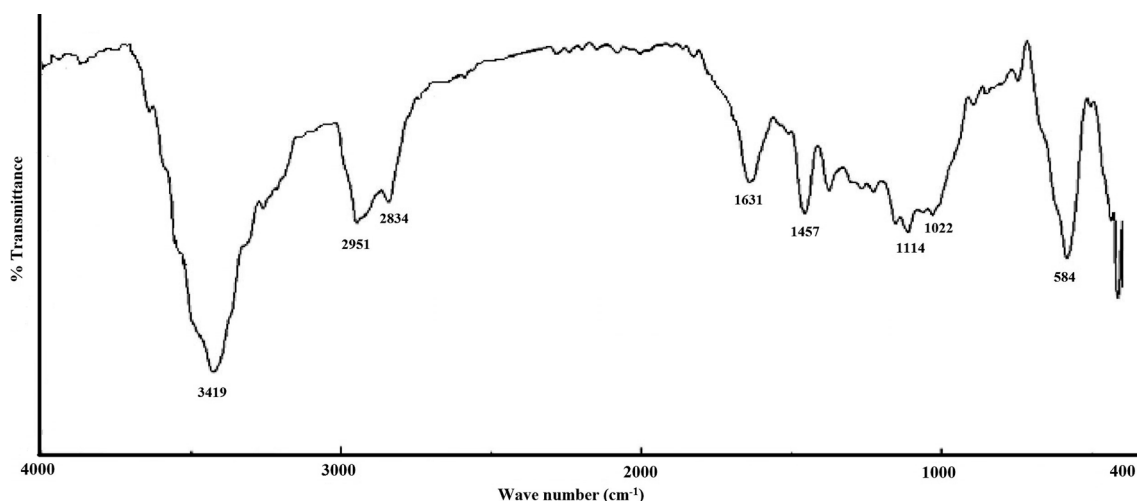


**Fig. 4** The FTIR spectrum of Fe@HPEI

stretching vibration [29]. These peaks demonstrate that the HPEI has been successfully coated on  $\text{Fe}_3\text{O}_4$ .

#### VSM Analysis

According to Fig. 5, the specific saturation magnetization of the  $\text{Fe}_3\text{O}_4$  and  $\text{Fe}_3\text{O}_4$ @HPEI is about 59.16 and 32.1 emu/g, respectively. Furthermore, no remanence and magnetic hysteresis loop confirm the superparamagnetic character of the synthesized adsorbents. Due to the existence of polyethyl-amine, which has no magnetic properties, on the surface of  $\text{Fe}_3\text{O}_4$ ,  $\text{Fe}_3\text{O}_4$ @HPEI has less specific saturation magnetization than  $\text{Fe}_3\text{O}_4$ . Our results indicated that  $\text{Fe}_3\text{O}_4$  and Fe@HPEI nanoparticles can be removed from the solution using a permanent magnet in short times of 15 and 25 s, respectively.

#### Central Composite Design

In current work, based on the CCD, thirty-nine experiments were determined for studying the influence of different parameters on dye adsorption by Fe@HPEI. In Table 2, the level of parameters, and experimental and predicted results of the RB 19 dye adsorption by Fe@HPEI are given. Table 2 and Fig. 6 show the predicted results were in good correspondence with the experimental results, which confirms the selected quadratic model is acceptable for the forecasting of dye adsorption. The internally studentized residuals against run numbers are shown in Fig. 7. This figure confirms the data values are pointed in the favorable range of 3 and  $-3$  [30], and the residuals are randomly distributed close to the center line. These data indicate the normal distribution of errors and the suitability of the model.

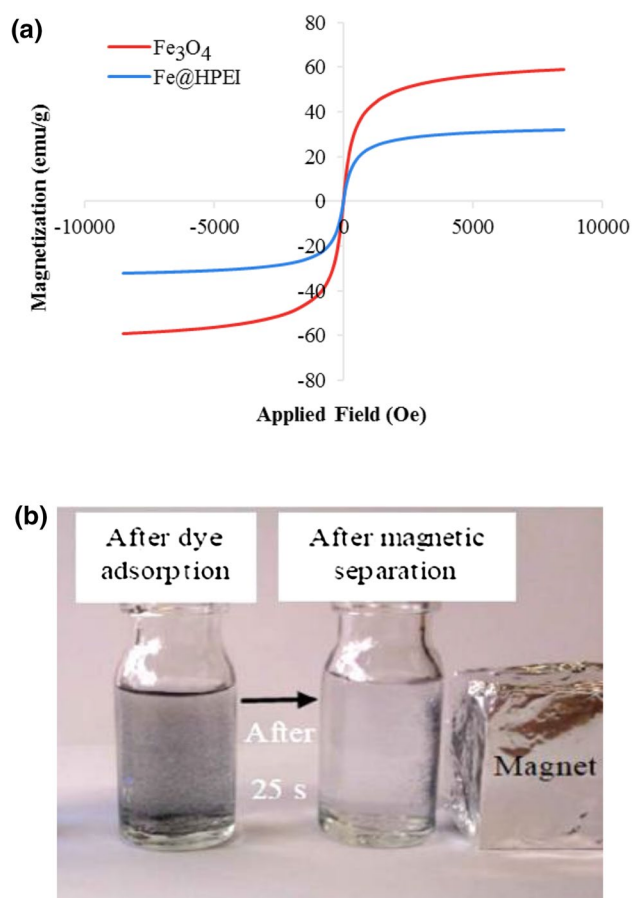


**Fig. 5** **a** Hysteresis loop of  $\text{Fe}_3\text{O}_4$  and Fe@HPEI, and **b** photographs of dye solution after dye adsorption and after magnetic separation

**Table 2** Central composite design matrix for RB 19 dye adsorption

Run order	pH	Level of variables			Response (Dye adsorption%)		Residual	$q_e$ (mg/g)
		Adsorbent dose (g/L)	Time (min)	Dye concentration (mg/L)	Experimental	Predicted		
1	9	0.2	23	65	67.61	69.76	-2.15	219.75
2	7	0.5	16	110	98.21	94.26	3.95	216.07
3	7	0.3	16	110	84.96	80.94	4.02	311.52
4	9	0.4	23	65	96.39	93.69	2.7	156.63
5	7	0.3	16	110	83.95	80.94	3.01	307.81
6	7	0.3	16	110	79.82	80.94	-1.12	292.7
7	5	0.4	23	65	99.78	107.56	-7.78	162.14
8	9	0.4	9	65	93	90.29	2.71	151.12
9	7	0.3	16	110	84.27	80.94	3.33	308.9
10	7	0.3	16	110	83.33	80.94	2.39	305.56
11	11	0.3	16	110	58.2	60.45	-2.25	213.4
12	5	0.2	23	65	89.06	85.09	3.97	289.44
13	7	0.3	16	200	50.13	49.33	0.8	334.2
14	5	0.2	9	65	79.1	76.74	2.36	254.08
15	5	0.4	9	65	96.83	98.39	-1.56	157.34
16	7	0.3	16	110	80.11	80.94	-0.83	293.6
17	5	0.2	23	155	55.12	59.27	-4.15	427.07
18	5	0.2	9	155	47.15	49.18	-2.03	365.44
19	7	0.3	16	110	76.87	80.94	-4.07	281.8
20	9	0.2	23	155	42.54	40.31	2.23	329.69
21	7	0.3	16	110	83.04	80.94	2.1	304.5
22	5	0.4	9	155	78.21	77.51	0.7	303.07
23	3	0.3	16	110	90.54	87.51	3.03	331.99
24	7	0.3	16	20	99.64	99.66	-0.02	66.42
25	7	0.3	16	110	82.12	80.94	1.18	301.1
26	7	0.3	16	110	78.54	80.94	-2.4	288
27	7	0.3	2	110	68.14	70.65	-2.51	249.85
28	9	0.4	9	155	62.49	65.78	-3.29	242.16
29	7	0.3	16	110	84.44	80.94	3.5	309.6
30	7	0.3	16	110	82.45	80.94	1.51	302.3
31	9	0.2	9	65	66.19	67.17	-0.98	215.13
32	7	0.3	30	110	87.43	84.15	3.28	320.59
33	9	0.2	9	155	42.31	35.98	6.33	327.87
34	7	0.3	16	110	75.04	80.94	-5.9	275.2
35	5	0.4	23	155	90.07	88.42	1.65	349.02
36	7	0.3	16	110	78.51	80.94	-2.4	287.85
37	7	0.1	16	110	38.82	42	-3.18	427.05
38	9	0.4	23	155	67.11	70.92	-3.81	260.04
39	7	0.3	16	110	76.68	80.94	-4.26	281.16

## Analysis of Variance

The analysis of variance data for the adsorption of RB 19 dye is presented in Table 3. In this table, P value less than 0.05 suggests the effect of parameters and models items are significant [31, 32]. To judge about the model

adequacy, the P value [33], lack of fit and  $R^2$  were considered [34]. The model P value 0.0002,  $R^2$  0.989, and lack of fit higher than 0.05 demonstrate the high significance of polynomial model for RB 19 dye adsorption by Fe@HPEI. Analysis of variance showed the significant influence of all selected independent variables on dye adsorption (P

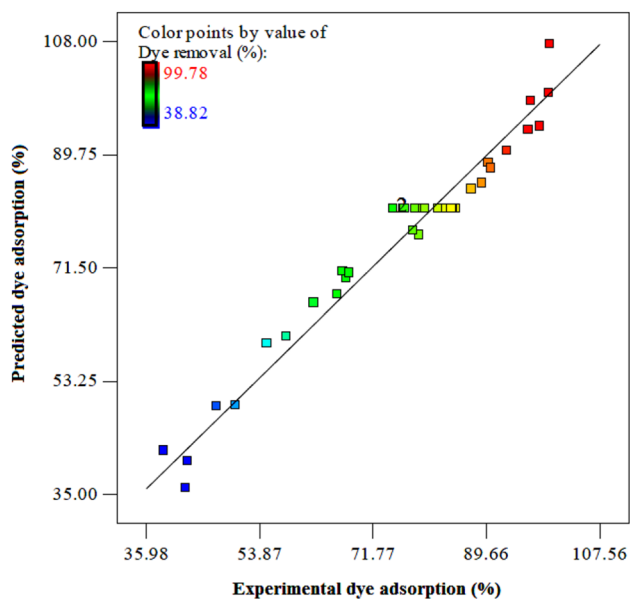


**Fig. 6** Plot of predicted data versus experimental RB 19 dye adsorption onto Fe@HPEI

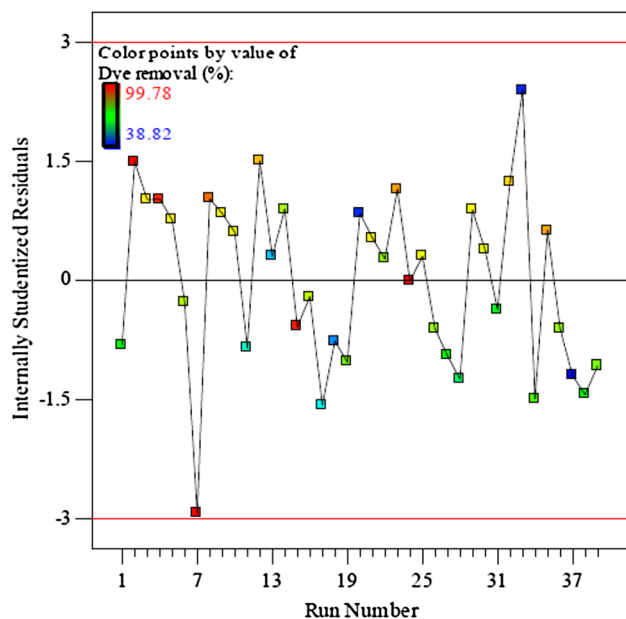


**Fig. 7** Distribution of residual data for dye adsorption using Fe@HPEI

value  $< 0.05$ ) [35]. The highest F value of 244 which is related to the effect of adsorbent dose on dye adsorption indicating the adsorbent dose is the most effective variable in dye adsorption. According to the results, the interaction effect of independent variables was insignificant.

**Table 3** ANOVA data for RB 19 dye adsorption by Fe@HPEI

Source	Sum of squares	Degrees of freedom	Mean square	F value	Prob > F
Model	9967.06	14	711.93	42.46	<0.0001
A	1098.37	1	1098.37	65.51	<0.0001
B	4097.18	1	4097.18	244.38	<0.0001
C	273.24	1	273.24	16.3	0.0005
D	3799.66	1	3799.66	226.64	<0.0001
AB	2.16	1	2.16	0.13	0.7227
AC	33.29	1	33.29	1.99	0.1716
AD	13.18	1	13.18	0.79	0.3831
BC	0.66	1	0.66	0.039	0.8448
BD	44.62	1	44.62	2.66	0.1159
CD	3.03	1	3.03	0.18	0.6747
A <sup>2</sup>	100.22	1	100.22	5.98	0.0222
B <sup>2</sup>	339.77	1	339.77	20.27	0.0001
C <sup>2</sup>	26	1	26	1.55	0.2251
D <sup>2</sup>	85.94	1	85.94	5.13	0.0329
Residual	402.37	24	16.77		
Lack of fit	257.03	10	25.7	2.48	0.0592
Pure error	145.34	14	10.38		
Cor total	10369.43	38			

$$R^2 = 0.9612, \text{ Adjusted } R^2 = 0.9386$$

Based on the regression coefficients, the empirical relationship between the dye adsorption and independent variables is presented as follows:

$$\begin{aligned} \text{Dye adsorption (\%)} = & 80.46 - 6.76A + 13.07B + 3.37C \\ & - 12.58D - 1.77A^2 - 3.23B^2 - 1.64D^2 \end{aligned} \quad (2)$$

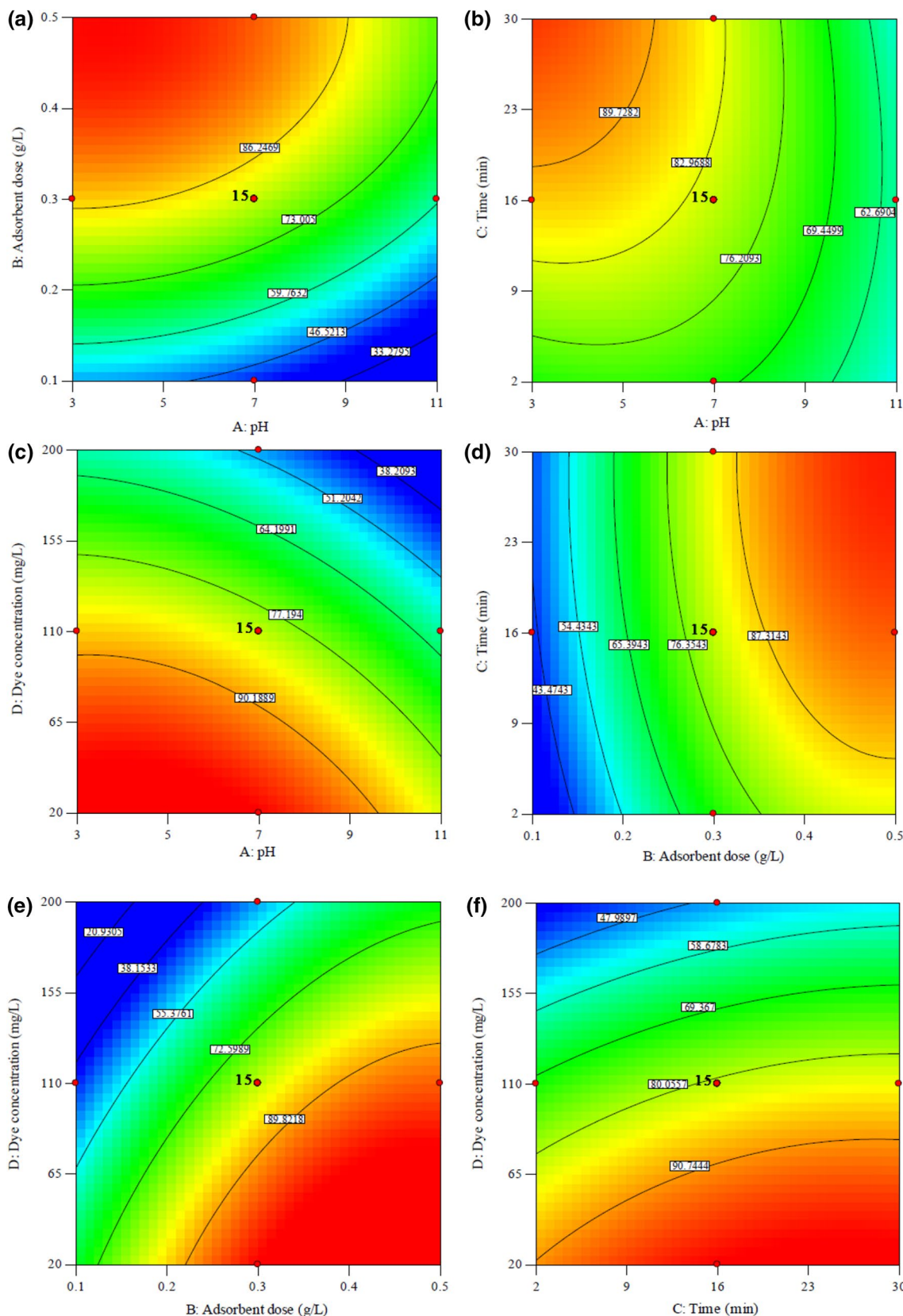
where A, B, C, and D are the coded values of pH, adsorbent dose, contact time and dye concentration, respectively.

Coefficients in Eq. 2 indicating the positive effect of adsorbent dose and contact time, and the negative effect of pH and initial dye concentration on dye adsorption.

### The Effect of Independent Variables on Dye Adsorption

Figure 8 illustrates how the independent variables affect RB 19 dye adsorption. Figure 8a, d, e reveals, by raising Fe@HPEI dose from 0.1 to 0.5 g/L, dye removal was enhanced and the maximum dye removal efficiency was attained at the adsorbent dose of 0.5 g/L and acidic pH of 3. When the adsorbent dose grows due to the existence of more available adsorption sites dye removal enhances [36].

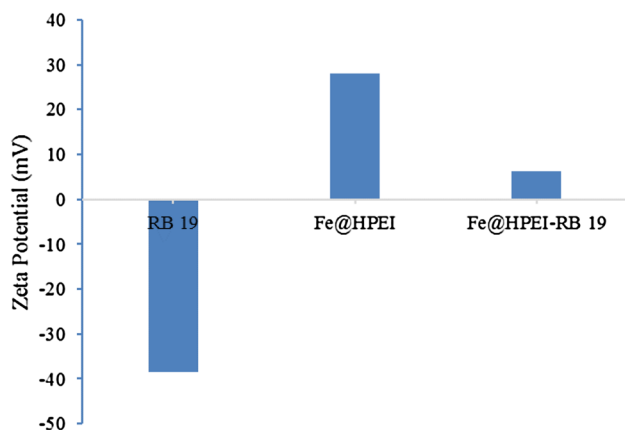
Based on Fig. 8a, b, c, raising pH from 3 to 11 lead to decreasing dye adsorption. This result can be explained by studying the zeta potential of adsorbent and dye solution.



**Fig. 8** Two-dimensional contour plots showing the effect of independent variables on RB 19 dye adsorption efficiency: **a** A–B, dye concentration 110 mg/L, time 16 min; **b** A–C, dye concentration

110 mg/L, adsorbent dose 0.3 g/L; **c** A–D, adsorbent dose 0.3 g/L, time 16 min; **d** B–C, dye concentration 110 mg/L, pH 7; **e** B–D, time 16 min, pH 7; **f** C–D, adsorbent dose 0.3 g/L, pH 7





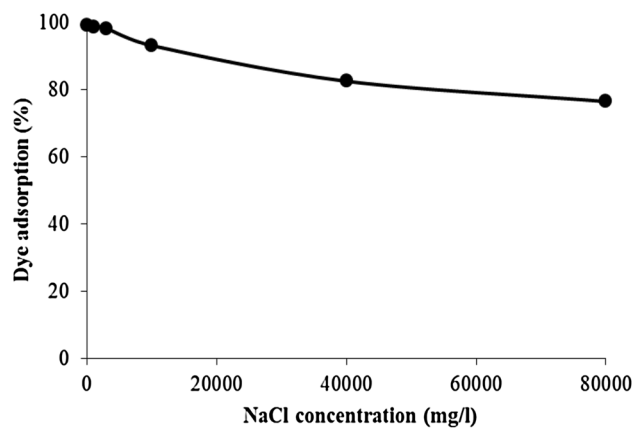
**Fig. 9** Zeta potential of the solutions containing RB 19, Fe@HPEI, and Fe@HPEI-RB 19

Figure 9 shows the zeta potential of the dye solution and the zeta potential of Fe@HPEI before and after dye adsorption. The zeta potential of dye solution containing 113 mg/L RB 19 was found to be  $-38.4$  mV that indicates RB 19 has the negative charge. The zeta potential of Fe@HPEI was  $+28$  mV at pH 3.4, while after dye adsorption it reduced to  $+6.36$  mV.

Higher dye removal at lower pH can be described by the fact that, at lower pH because of the existence of higher amounts of  $H^+$  ions in the solution more amine groups are protonated and the protonated amines on the surface of Fe@HPEI which have positive charge can effectively adsorb negatively charged RB 19 dye molecules containing sulfonate groups by electrostatic interaction. The similar interaction has been suggested for the adsorption of an anionic dye (Reactive Brilliant Red K-2BP) by amine functionalized walnut shell [37].

Figure 8c, e, f shows that an increase in dye concentration from 20 to 200 mg/L lead to a dramatic decline in dye adsorption. In a specific dose of adsorbent, the number of active adsorption sites is limited [38]. Thus, with increasing dye concentration the number of active sites for the adsorption of all dye molecules is not enough and eventually the percentage of dye adsorption decreases.

According to Fig. 8b, d, f increasing contact time from 2 to 30 min cause the rise of the RB 19 dye adsorption. It has been established that sufficient contact time provides an opportunity for interaction between the adsorbate and the adsorbent. So, contact time has a positive effect on dye adsorption. The similar trends have been reported for the adsorption of anionic dye congo red onto modified hectorite [39], and arsenate adsorption onto MWCNT/MnO<sub>2</sub> [40]. In regards to the ANOVA results, the interaction effect between the whole independent variables was statistically insignificant.



**Fig. 10** Effect of ionic strength on dye adsorption (dye concentration: 113 mg/L, adsorbent dose: 0.4 g/L, pH 3.4, contact time: 25 min)

### Optimization

The main goal of optimization was to find out the optimal conditions to attain the highest dye adsorption. The contact time 25 min, pH 3.4, adsorbent dose 0.4 g/L, and the initial dye concentration of 113 mg/L were suggested by Design Expert software as the optimal values to reach the highest dye adsorption efficiency of 100%, while the independent variables were adjusted to the studied range. According to our results, the average experimental dye adsorption of 99.27%, which is resulted from the performing of experiments in triplicate at optimum conditions is near to the predicted value of 100% affirms the validity of the model. In optimum conditions, the efficiency of dye removal by the Fe@HPEI was compared to Fe<sub>3</sub>O<sub>4</sub> and the results revealed the Fe@HPEI was 3.6 times more efficient than that of Fe<sub>3</sub>O<sub>4</sub>.

### Influence of Ionic Strength

Textile wastewaters commonly contain a high concentration of salts and have high ionic strength, which can influence the adsorption of pollutant molecules on the adsorbent. In order to assess the effect of ionic strength on dye adsorption efficiency, NaCl that is the most commonly used salt in textile industries [41] was added to the colored solution at various concentrations of 1000, 3000, 10,000, 40,000 and 80,000 mg/L, similar to salt concentration in real textile wastewater. Figure 10 shows a decrease in dye adsorption by increasing the salt concentration from 0 to 80,000 mg/L. These results can be explained by this fact that the salt molecules can occupy adsorption sites onto the adsorbent. Moreover, chloride anions existed in the solution may also compete with negatively charged dye molecules for adsorption onto the adsorbent surface, which leads to a decrease in dye adsorption [41].

### Reusability of Fe@HPEI

In view of economic aspect, it is very important for an adsorbent to be reusable [36] and for its regeneration process to be easy. In regeneration process, the pollutants which are adsorbed onto the adsorbent desorb from the adsorbent and release into the solution.

For conducting desorption process, RB 19 dye loaded Fe@HPEI was mixed with 50 mL deionized water containing 0.1 M NaOH for 30 min, and this process repeated three times. To eliminate excess NaOH, the regenerated nanoparticles were washed with deionized water for three times. The regenerated Fe@HPEI was employed for several times in the adsorption/desorption processes, and the data are given in Fig. 11. According to the figure, after five runs the dye adsorption efficiency declines from 99.27 to 76.1%. These data confirm that the prepared Fe@HPEI as an efficient adsorbent can be repeatedly used for the adsorption of dye.

### Adsorption Kinetic

To understand the rate of adsorption [42], a lot of kinetic models have been proposed. The results obtained from kinetic studies would be necessary for designing an adsorption system [36]. The kinetics of dye adsorption on Fe@HPEI were tested using the most practiced models which are pseudo-first-order, pseudo-second-order, and intraparticle diffusion models (applicable model is shown in Fig. 12).

The pseudo-first-order kinetic is expressed by the following equation [43, 44]:

$$\log(q_e - q_t) = \log q_e - \frac{k_1 t}{2.303} \tag{3}$$

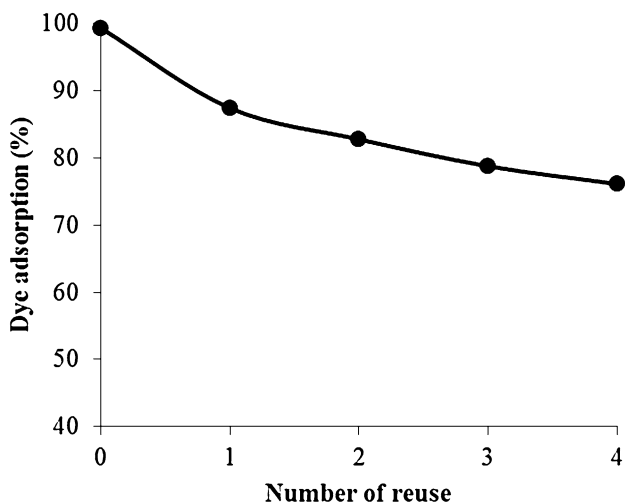


Fig. 11 Reuse of Fe@HPEI nanoparticles (dye concentration: 113 mg/L, adsorbent dose: 0.4 g/L, pH 3.4, contact time: 25 min)

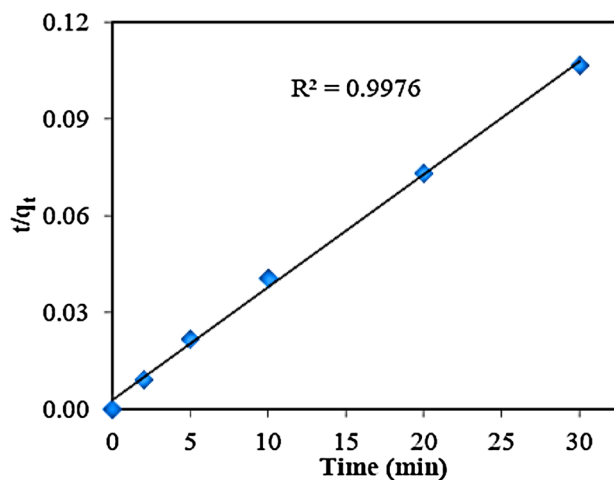


Fig. 12 Plot of Pseudo-second-order kinetic for RB 19 dye adsorption on Fe@HPEI (dye concentration: 113 mg/L, adsorbent dose: 0.4 g/L, pH 3.4)

where  $q_e$  (mg/g),  $q_t$  (mg/g),  $k_1$  ( $\text{min}^{-1}$ ) and  $t$  (min) are the amount of adsorbed dye on adsorbent at the equilibrium, the amount of adsorbed dye at time  $t$ , the pseudo-first-order rate constant and time of reaction, respectively.  $K_1$  and  $q_e$  were calculated from the slope and intercept of the linear plot of  $\log(q_e - q_t)$  versus time of reaction, respectively.

The adsorption data were tested using pseudo-second-order model. This model is given as follows [45, 46]:

$$\frac{t}{q_t} = \frac{1}{k_2 q_e^2} + \frac{t}{q_e} \tag{4}$$

where  $k_2$  (g/mg min) is the pseudo-second-order rate constant. The slope and intercept of the linear plot of  $t/q_t$  versus  $t$  were used to determine  $q_e$  and  $k_2$ , respectively.

The adsorption kinetic was also described by intraparticle diffusion model. This model assumes that film diffusion is negligible and intraparticle diffusion is the only rate-controlling step in the adsorption process [47]. During the intraparticle diffusion process, the adsorbate species are transferred from the solution into the solid phase. The intraparticle diffusion model is shown by the Eq. (5):

$$q_t = k_{id} t^{1/2} + C \tag{5}$$

where  $k_{id}$  ( $\text{mg/g min}^{1/2}$ ) is the intraparticle diffusion rate constant.  $k_{id}$  and  $C$  were determined from the slope and intercept of the linear plot of  $q_t$  against  $t^{1/2}$ . The value of  $C$  describes the thickness of the boundary layer [48]. The larger intercept, the greater boundary layer effect.

In Table 4, the kinetic data for dye adsorption onto Fe@HPEI are listed. Based on the highest correlation coefficient, the adsorption data were fitted well with the pseudo-second-order model ( $R^2 = 0.997$ ).

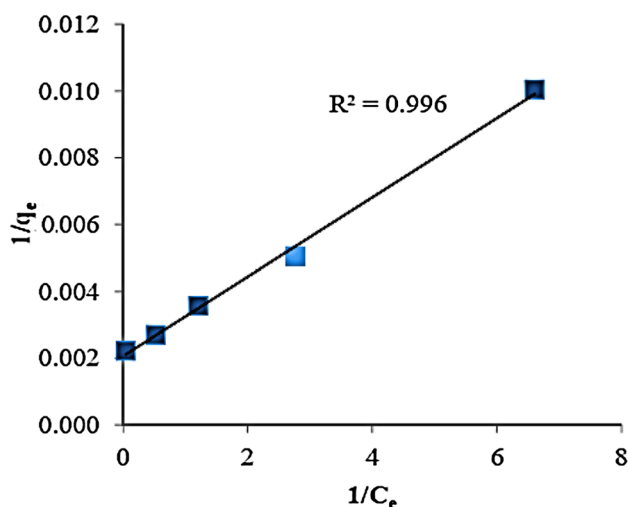
**Table 4** The values of kinetic constants for the adsorption of RB 19 dye on Fe@HPEI

Kinetic	Kinetic constant	Value
Pseudo-first-order	$k_1$ ( $\text{min}^{-1}$ )	0.07
	$q_e$ (mg/g)	3.8
	$R^2$	0.18
Pseudo-second-order	$k_2$ (g/mg min)	0.0045
	$q_e$ (mg/g)	285.7
	$R^2$	0.997
Intraparticle diffusion	$k_{ip}$ (mg/g $\text{min}^{1/2}$ )	43.4
	$C$ (mg/g)	87.02
	$R^2$	0.69

The value of  $q_e$  experimental was 281.5 mg/g. Thus, the value of  $q_e$  computed using pseudo-second-order model is close to  $q_e$  obtained from experimental data.

### Adsorption Isotherm

The relationship between the amount of pollutant adsorbed onto the adsorbent and equilibrium concentration of the pollutant in solution at a specific temperature is defined as the adsorption isotherm. The adsorption capacity of each and every adsorbent can be calculated by the use of an appropriate adsorption isotherm [49]. In the present work, the adsorption isotherms were described by the Langmuir, Freundlich and Temkin models (applicable model is presented in Fig. 13), and adsorption parameters are presented in Table 5. The adsorption isotherm experiments were carried at the optimal conditions which were the initial adsorbent dose of 0.4 g/L, time 25 min, pH 3.4 at various initial dye concentrations of 40, 80, 113, 150

**Fig. 13** Plot of Langmuir isotherm for RB 19 dye adsorption on Fe@HPEI (adsorbent dose: 0.4 g/L, pH 3.4, contact time: 25 min)**Table 5** The values of Isotherm parameters for the adsorption of RB 19 dye on Fe@HPEI

Isotherm	Isotherm parameter $q_{\text{max}}$ (mg/g)	Value 500
Langmuir	$b$ (L/mg)	1.66
	$R_L$	0.8
	$R^2$	0.996
	$K_F$ (mg/g) (L/mg) <sup>1/n</sup>	240.43
Freundlich	$n$	3.49
	$R^2$	0.8
Temkin	$b$ (kJ/mol)	108.96
	$A$ (1/g)	45.43
	$R^2$	0.92

and 200 mg/L. The applicability of the isotherm equations to the equilibrium data were judged by the value of the correlation coefficients ( $R^2$ ).

The Langmuir isotherm model assumes that the monolayer sorption takes place onto a homogeneous adsorbent surface with a limited number of identical sites [50, 51]. The linear form of Langmuir isotherm is given by the following equation [52]:

$$\frac{1}{q_e} = \frac{1}{q_{\text{max}}} + \frac{1}{bq_{\text{max}}} \frac{1}{C_e} \quad (6)$$

where  $q_e$  (mg/g) and  $C_e$  (mg/L) are the mass of dye adsorbed per unit mass of adsorbent and the equilibrium concentration of dye, respectively.  $q_{\text{max}}$  (mg/L) is the maximum monolayer sorption capacity at equilibrium,  $b$  (L/mg) is the Langmuir constant. The  $b$  and  $q_{\text{max}}$  can be determined from the plot of  $1/C_e$  against  $1/q_e$ .

The following equation represents the Langmuir separation factor that is a dimensionless constant:

$$R_L = \frac{1}{(1 + bC_0)} \quad (7)$$

where  $C_0$  (mg/L) and  $b$  (L/mg) are the highest initial dye concentration and the Langmuir constant. The  $R_L$  value shows the nature of adsorption. The value of  $R_L > 1$ ,  $R_L = 1$ ,  $0 < R_L < 1$  or  $R_L = 0$  suggests that the adsorption process is unfavorable, linear, favorable, or irreversible, respectively [53].

The Freundlich isotherm describes the multilayer coverage of adsorbate on heterogeneous adsorbent surface sites with different binding energies [49]. The linear form of Freundlich isotherm can be written as follows:

$$\log q_e = \log k_f + \frac{1}{n} \log C_e \quad (8)$$

where  $K_f$  (mg/g)  $(l/mg)^{1/n}$  is the Freundlich adsorption capacity constant,  $n$  (dimensionless) is the Freundlich adsorption intensity parameter.  $K_f$  and  $n$  can be evaluated from the intercept and slope of the linear plot of  $\log q_e$  versus  $\log C_e$ .

In order to judge about the affinity of the adsorbent surface toward pollutant, the Temkin model was used. The linear form of Temkin isotherm is given by the Eq. (9) [54]:

$$q_e = \frac{RT}{b} \ln A + \frac{RT}{b} \ln C_e \tag{9}$$

where  $R$  (8.314 J/mol K) and  $T$  ( $^{\circ}k$ ) are universal gas constant and temperature, respectively.  $A$  and  $b$  which are Temkin isotherm constants can be obtained from the intercept and slope of the linear plot of  $q_e$  versus  $\ln C_e$ , respectively.

From Table 5, the highest correlation coefficient of 0.996 which corresponds to Langmuir isotherm suggests that the adsorption of RB 19 onto Fe@HPEI is monolayer and homogeneous [55].

Moreover, the  $R_L$  value of 0.8 which is between 0 and 1 affirms that the dye adsorption process onto Fe@HPEI is favorable [56].

### Thermodynamic Study

To assess the influence of solution temperature on dye removal and evaluate the feasibility of RB 19 dye adsorption onto Fe@HPEI the thermodynamic study was carried out at temperatures ranged from 280 to 323  $^{\circ}K$  (Fig. 14a). Thermodynamic parameters, such as enthalpy change ( $\Delta H^{\circ}$ ), Gibbs free energy change ( $\Delta G^{\circ}$ ) and entropy change ( $\Delta S^{\circ}$ ) were computed according to the following equations [57]:

$$\Delta G^{\circ} = RT \ln K_l \tag{10}$$

$$\ln k_l = \frac{\Delta S^{\circ}}{R} - \frac{\Delta H^{\circ}}{RT} \tag{11}$$

where  $K_l$ ,  $R$  (8.314 J/K mol) and  $T$  ( $^{\circ}K$ ) are equilibrium distribution constant, universal gas constant and temperature, respectively.  $\Delta H^{\circ}$  and  $\Delta S^{\circ}$  were calculated from the slope and intercept of  $\ln K_l$  against  $1/T$  (Fig. 14b) [58].

From Table 6, the negative values of  $\Delta G^{\circ}$  in all temperatures confirm the spontaneous nature of dye adsorption onto the adsorbent [52, 59]. An increase in dye removal with increasing temperature indicates the endothermic nature of adsorption. Furthermore, the positive value of  $\Delta H^{\circ}$  implies that the adsorption process is endothermic [57, 60]. The positive value of  $\Delta S^{\circ}$  reflects the affinity of Fe@HPEI for RB 19 dye [61].

### Comparison of Fe@HPEI with Other Adsorbents

The efficiency of Fe@HPEI for RB 19 dye adsorption was compared with other adsorbents and the results are represented in Table 7. The data in Table 7 indicate that acidic pH is the most favorable pH for the adsorption of RB 19. Compared to activated carbon and other adsorbents, Fe@HPEI, in term of adsorption capacity, has a higher potential to remove RB 19 from aqueous solution.

**Table 6** Thermodynamic parameters for dye adsorption by Fe@HPEI

Parameter	Temperature ( $^{\circ}K$ )	$\Delta G^{\circ}$ (kJ/mol)	$\Delta H^{\circ}$ (kJ/mol)	$\Delta S^{\circ}$ (J/mol k)
Value	280	-6.35	92.28	355
	288	-10.95		
	298	-14.44		
	308	-17.03		
	323	-22.19		

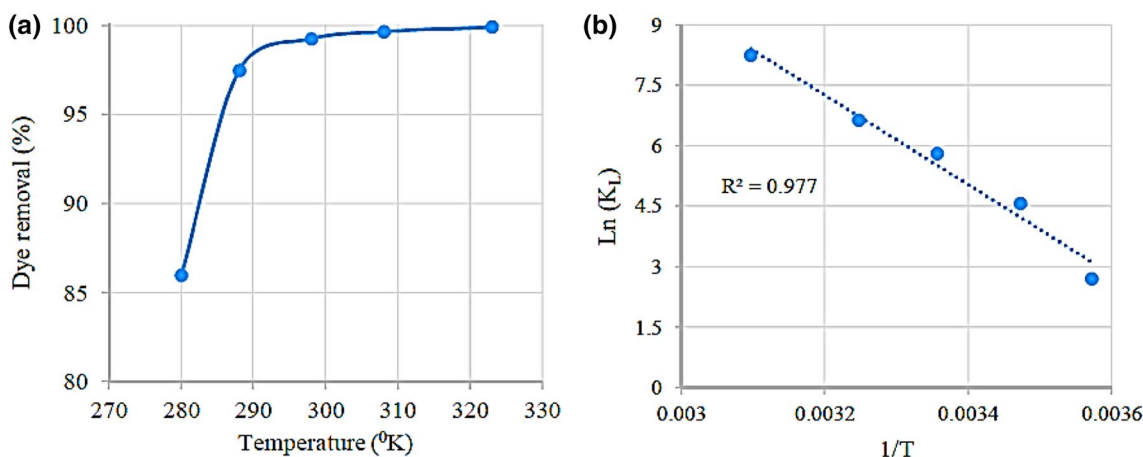


**Fig. 14** a Influence of temperature on dye removal, and b plot of  $\ln K_l$  versus  $1/T$

**Table 7** Comparison of various adsorbents for RB 19 adsorption

Adsorbent	Maximum adsorption capacity (mg/g)	pH	Applicable kinetic model	Applicable isotherm model	References
Furnace slag	60	2	Pseudo-first-order	Langmuir	[62]
Wheat bran	117	1.5	Pseudo-second-order	Langmuir	[63]
Modified bentonite with a cationic surfactant (DTMA)	206.5	1.5	Pseudo-second-order	Langmuir	[64]
Seawater neutralized red mud	416.7	4	Pseudo-second-order	Langmuir	[65]
Coconut shell based activated carbon	2.2	6.2	Pseudo-second-order	Langmuir	[52]
Diethylenetriamine functionalized magnetic chitosan	109.14	2	Pseudo-second-order	Langmuir	[66]
Polypyrrole-coated magnetic nanoparticles	112.36	3	Pseudo-second-order	Langmuir	[67]
Fe <sub>3</sub> O <sub>4</sub> @L-arginine	125	3	Pseudo-second-order	Freundlich	[20]
Fe@HPEI	500	3.4	Pseudo-second-order	Langmuir	This study

## Conclusion

Fe@HPEI nanoparticle as an appropriate super adsorbent was synthesized, characterized, and repeatedly utilized for RB 19 dye adsorption in different operational conditions. The statistical analysis indicated adsorbent dose and contact time had a positive effect on dye adsorption, while pH and initial dye concentration showed a negative effect. The optimum conditions to reach the highest predicted dye adsorption of 100% were suggested to be pH 3.4, contact time 25 min, the adsorbent dose of 0.4 g/L and the initial dye concentration of 113 mg/L. At optimal condition the maximum dye adsorption 99.27% was attained. The RB 19 dye adsorption data were fitted well to the pseudo-second-order kinetic and the Langmuir isotherm, and the nature of adsorption was endothermic.

**Acknowledgements** The authors are grateful to Center for Water Quality Research, Tehran University of Medical Sciences for financial support of this study (Grant Number: 94-01-46-28904). The first author would like to thank, Shahid Sadoughi University of Medical Sciences for supporting current work.

## Compliance with Ethical Standards

**Conflict of interest** The authors declare that they have no conflict of interest.

## References

- Gholami-Borujeni F, Mahvi AH, Nasseri S, Faramarzi MA, Nabizadeh R, Alimohammadi M (2011) *Appl Biochem Biotechnol* 165:1274–1284
- Wang T, Kailasam K, Xiao P, Chen G, Chen L, Wang L, Li J, Zhu J (2014) *Microporous Mesoporous Mater* 187:63–70
- Mahmoodi NM, Dalvand A (2013) *Desalin Water Treat* 51:5959–5964
- Maleki A, Mahvi AH, Ebrahimi R, Zandsalimi Y (2010) *Korean J Chem Eng* 27:1805–1810
- Yousefi N, Nabizadeh R, Nasseri S, Khoobi M, Nazmara S, Mahvi AH (2017) *Korean J Chem Eng* 34:2342–2353
- Nematollahzadeh A, Shojaei A, Karimi M (2015) *React Funct Polym* 86:7–15
- Natarajan S, Bajaj HC, Tayade RJ (2018) *J Environ Sci* 65:201–222
- Tsang DC, Hu J, Liu MY, Zhang W, Lai KC, Lo IM (2007) *Water Air Soil Pollut* 184:141–155
- Khatri A, Peerzada MH, Mohsin M, White M (2015) *J Clean Prod* 87:50–57
- Klemola K, Honkalampi-Hämäläinen U, Liesivuori J, Pearson J, Lindström-Seppä P (2006) *Autex Res J* 6:182–190
- Dalvand A, Gholami M, Joneidi A, Mahmoodi NM (2011) *Clean-Soil Air Water* 39:665–672
- Dalvand A, Gholibegloo E, Ganjali MR, Golchinpoor N, Khazaei M, Kamani H, Hosseini SS, Mahvi AH (2016) *Environ Sci Pollut Res* 23:16396–16405
- Fathy NA, El-Shafey SE, El-Shafey OI, Mohamed WS (2013) *J Environ Chem Eng* 1:858–864
- Ergene A, Ada K, Tan S, Katurcioglu H (2009) *Desalination* 249:1308–1314
- Shirmardi M, Mahvi AH, Hashemzadeh B, Naeimabadi A, Hassani G, Niri MV (2013) *Korean J Chem Eng* 30:1603–1608
- Mohammadi N, Khani H, Gupta VK, Amereh E, Agarwal S (2011) *J Colloid Interface Sci* 362:457–462
- Cao D, Jin X, Gan L, Wang T, Chen Z (2016) *Chemosphere* 159:23–31
- Yoon SU, Mahanty B, Ha HM, Kim CG (2016) *J Nanopart Res* 18:1–10
- Li DP, Zhang YR, Zhao XX, Zhao BX (2013) *Chem Eng J* 232:425–433
- Dalvand A, Nabizadeh R, Ganjali MR, Khoobi M, Nazmara S, Mahvi AH (2016) *J Magn Magn Mater* 404:179–189
- Zhang YR, Shen SL, Wang SQ, Huang J, Su P, Wang QR, Zhao BX (2014) *Chem Eng J* 239:250–256
- Xia T, Guan Y, Yang M, Xiong W, Wang N, Zhao S, Guo C (2014) *Colloids Surf A* 443:552–559
- Chen CT, Wang LY, Ho YP (2011) *Anal Bioanal Chem* 399:2795–2806
- Sajab MS, Chia CH, Zakaria PS, Khiew SC (2013) *Bioresour Technol* 128:571–577
- Sun XF, Wang SG, Cheng W, Fan M, Tian BH, Gao BY, Li XM (2011) *J Hazard Mater* 189:27–33
- Kim MH, Hwang CH, Kang SB, Kim S, Park SW, Yun YS, Won SW (2015) *Chem Eng J* 280:18–25
- Liu J, Ma S, Zang L (2013) *Appl Surf Sci* 265:393–398

28. Khoobi M, Delshad TM, Vosooghi M, Alipour M, Hamadi H, Alipour E, Hamedani MP, Safaei Z, Foroumadi A, Shafiee A (2015) *J Magn Magn Mater* 375:217–226
29. Pang Y, Zeng G, Tang L, Zhang Y, Liu Y, Lei X, Li Z, Zhang J, Xie G (2011) *Desalination* 281:278–284
30. Ashrafi S, Nasser S, Alimohammadi M, Mahvi A, Faramarzi M (2016) *Desalin Water Treat* 57:1–10
31. Ye J, Cong X, Zhang P, Zeng G, Hoffmann E, Liu Y, Wu Y, Zhang H, Fang W, Hahn HH (2016) *J Environ Manag* 167:1–7
32. Sahu MK, Sahu UK, Patel RK (2015) *RSC Adv* 5:42294–42304
33. Zarei H, Nasser S, Nabizadeh R, Shemirani F, Dalvand A, Mahvi AH (2017) *Desalin Water Treat* 67:196–205
34. Kütahyalı C, Çetinkaya B, Acar MB, Işık NO, Cireli I (2012) *J Hazard Mater* 201:115–124
35. Fakhri A, Rashidi S, Tyagi I, Agarwal S, Gupta VK (2016) *J Mol Liq* 214:378–383
36. Zhu HY, Fu YQ, Jiang R, Jiang JH, Xiao L, Zeng GM, Zhao SL, Wang Y (2011) *Chem Eng J* 173:494–502
37. Cao JS, Lin JX, Fang F, Zhang MT, Hu ZR (2014) *Bioresour Technol* 163:199–205
38. Chang YP, Ren CL, Yang Q, Zhang ZY, Dong LJ, Chen XG, Xue DS (2011) *Appl Surf Sci* 257:8610–8616
39. Xia C, Jing Y, Jia Y, Yue D, Ma J, Yin X (2011) *Desalination* 265:81–87
40. Saleh TA, Agarwal S, Gupta VK (2011) *Appl Catal B* 106:46–53
41. Liu S, Ding Y, Li P, Diao K, Tan X, Lei F, Zhan Y, Li Q, Huang B, Huang Z (2014) *Chem Eng J* 248:135–144
42. Khosravi M, Azizian S (2014) *J Ind Eng Chem* 20:2561–2567
43. Xu C, Wang H, Yang W, Ma L, Lin A (2018) *J Polym Environ* 26:1206–1217
44. Zazouli MA, Mahvi AH, Dobaradaran S, Barafrashtehpour M, Mahdavi Y, Balarak D (2014) *Fluoride* 47:349–358
45. Yue L, Ge C, Feng D, Yu H, Deng H, Fu B (2017) *J Environ Sci* 57:180–189
46. Laabd M, El Jaouhari A, Bazzaoui M, Albourine A, El Jazouli H (2017) *J Polym Environ* 25:359–369
47. Ghaedi M, Hajjati S, Mahmudi Z, Tyagi I, Agarwal S, Maity A, Gupta V (2015) *Chem Eng J* 268:28–37
48. Sun L, Chen D, Wan S, Yu Z (2018) *J Polym Environ* 26:765–777
49. Rotte NK, Yerramala S, Boniface J, Srikanth VV (2014) *Chem Eng J* 258:412–419
50. Li H, An N, Liu G, Li J, Liu N, Jia M, Zhang W, Yuan X (2016) *J Colloid Interface Sci* 466:343–351
51. Saleh TA, Gupta VK (2014) *Adv Colloid Interface Sci* 211:93–101
52. Isah U, Abdulraheem G, Bala S, Muhammad S, Abdullahi M (2015) *Int Biodeter Biodegr* 102:265–273
53. Elsherbiny AS, El-Hefnawy ME, Gemeay AH (2018) *J Polym Environ* 26:411–422
54. Shekarriz M, Ramezani Z, Elhami F (2017) *Int J Environ Sci Technol* 14:1081–1090
55. Torkshavand Z, Gholami M, Farzadkia M, Esrafil A (2014) *Iran J Health Saf Environ* 1:101–110
56. Wang L, Zhao X, Zhang J, Xiong Z (2017) *Environ Sci Pollut Res* 24:14198–14206
57. Cui L, Wang Y, Gao L, Hu L, Yan L, Wei Q, Du B (2015) *Chem Eng J* 281:1–10
58. Gupta VK, Atar N, Yola ML, Üstündağ Z, Uzun L (2014) *Water Res* 48:210–217
59. Hassanpour S, Taghizadeh M, Yamini Y (2018) *J Polym Environ* 26:101–115
60. Karthikeyan S, Gupta V, Boopathy R, Titus A, Sekaran G (2012) *J Mol Liq* 173:153–163
61. Khademi Z, Ramavandi B, Ghaneian MT (2015) *J Environ Chem Eng* 3:2057–2067
62. Xue Y, Hou H, Zhu S (2009) *Chem Eng J* 147:272–279
63. Çiçek F, Özer D, Özer A, Özer A (2007) *J Hazard Mater* 146:408–416
64. Özcan A, Ömeroğlu Ç, Erdoğan Y, Özcan AS (2007) *J Hazard Mater* 140:173–179
65. De Souza KC, Antunes MLP, Couperthwaite SJ, Da Conceição FT, De Barros TR, Frost R (2013) *J Colloid Interface Sci* 396:210–214
66. Elwakeel K, El-Bindary A, Ismail A, Morshidy A (2016) *RSC Adv* 6:22395–22410
67. Shanehsaz M, Seidi S, Ghorbani Y, Shoja SMR, Rouhani S (2015) *Spectrochim Acta Part A* 149:481–486